Broadband and tunable bandgap guidance based on the ring-pattern liquid-filled photonic crystal fibers

Bing Sun,[1,2,3] Yaqi Wen,[1] Taiyu Bian,[1] Fei Li[1], Kaiming Zhou,[2] Zuxing Zhang,[1,4]

[1]*Advanced Photonic Technology Lab, College of Electronics and Optical Engineering, Nanjing University of Posts and Telecommunications, Nanjing 210023, China*
[2]*Aston Institute of Photonic Technologies, Aston University, Birmingham B4 7ET, UK*
[3]b.sun@njupt.edu.cn
[4]zxzhang@njupt.edu.cn

Received XX Month XXXX; revised XX Month, XXXX; accepted XX Month XXXX; posted XX Month XXXX (Doc. ID XXXXX); published XX Month XXXX

A ring-pattern liquid-filled photonic crystal fiber (*R*-LPCF) scheme, which the first-ring holes (the six holes adjacent to the core) are filled with high index inclusions, has been experimentally demonstrated to extend over a wide-guided spectral range. In such new fiber the bandgap-like core mode is investigated, among which the telecommunication bandgap exhibits confinement losses 5 orders of magnitude smaller than those of the corresponding fully liquid-filled photonic bandgap fibers. Besides, the *R*-LPCF serving the thermal tunability when filled with index-matching liquid, enables the guided bandwidth switching from 1.5-μm-band to 1.3-μm-band communication window. Moreover, the structural parameters for two commercial PCFs are quantified to confirm the feasibility of the proposed method. © 2021 Optical Society of America

Photonic crystal fibers (PCFs), which consists of an array of glass capillaries running along an entire fiber length, allow for the accessibility of the air channels for microscale functionalization (e.g., filling the index matched liquids [1], liquid crystals [2-3], metals [4], ferrofluids [5-6], polymers [7], glasses [8] into the air channels). Such infiltrating actions [9-12] can lead to the switch from the modified total internal reflection (MTIR) guidance to the photonic bandgap (PBG) guidance, then providing an attractive playground for in-fiber optical sensors. Wang et al. [11] investigated an invertible fiber-type transformation from a PBG fiber into an unideal waveguide and then into an index-guiding PCF via the thermo-optic effect of the fluid. Recently, we demonstrated a liquid-crystal-filled PCF and investigated its temperature response nearby a unique liquid crystal's clearing point [12]. It's undoubted that the fully fluid-filled PCFs are usually involved with large insertion loss, seriously limiting their performance. For instance, Zu et al. [6] reported a magnetic field sensor based on the bandgap tunability of the PCF by filling magnetic fluid with high refractive index while the insertion loss of this sensor is more than 50 dB.

As an alternative, many selective infiltration techniques (e.g., focused ion beam (FIB) milled microchannels [13], femtosecond laser-assisted (FL) technique [14-16], direct manual gluing (DMG) [17-19]) are used for decreasing the insertion loss, improving the fiber tunability, and then enhancing the sensitivity. Taking the DMG method as an example, typically under a microscope, a glass tip of submicrometer scale was used to drop UV curable polymers into air holes before blocking. The different glass tips were required for different air-hole sizes and when the diameter of the air-hole changes greatly in the cross-section of the PCF, substantial operation inconvenience was created. Referring to the FIB and femtosecond laser-assisted techniques, long milling time, expensive apparatus or sophisticated technologies were required. Besides, the fiber structures fabricated by the aforementioned selective-infiltration techniques just support finite spectral windows, leading to very unusual dispersive and spectral properties. By contrast, the PBG-guidance fibers are particularly interesting since they associate the advantages of bandgaps with the amazing optical properties of these fibers.

In this *Letter*, we propose a very simple, inexpensive selective infiltration technique to develop a ring-pattern liquid filled photonic crystal fibers (*R*-LPCF) against two commercial PCFs, where only the first-ring holes adjacent to the core exhibits inclusions with refractive index higher than the silica matrix while other outer rings still being composed by air holes. In contrast to the fully liquid filled PCF (*F*-LPCF), i.e., all air holes are filled with liquid, the proposed *R*-LPCF present a bandgap-like guided core mode strongly analogous to the fundamental mode of the *F*-LPCF however, serving wide spectral ranges and low confinement losses. Moreover, the *R*-LPCF corresponds to an analyte volume of approximately one sixth, it consequently contributes to a low insertion loss, which is no more

than 2 dB. Finally, properties of the *R*-LPCF by using two commercial PCFs of appropriate lengths and of different temperature environment are further investigated.

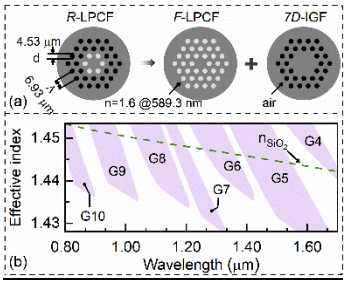

Fig. 1 (a) Cross sections of the *R*-LPCF and the corresponding *F*-LPCF and the *7D*-IGF. (b) Bandgap maps of the *R*-LPCF.

As outlined in Ref. [20], there would be no true bandgap defined in the *R*-LPCF but inducing a bandgap-like mode over a large spectral range with relatively low loss, the features of which presents significantly analogous to the true PBG fibers or other hybrid fibers. Conceptually similarly, the proposed *R*-LPCF can be decomposed into the *F*-LPCF with infinite periodic lattice and an index-guiding fiber with 7-defect core (*7D*-IGF). As shown in Fig. 1(a), we take advantage of the equivalent PBG model to evaluate the location of bandgap-like modes guided in the cladding unit cell, i.e., effective-index curves in the *R*-LPCF by means of a full-vectorial plane wave method. The material dispersion of the silica is considered using the Sellmeier equation [21]. The infiltrated liquid possesses a refractive index of 1.60 for 589.3 nm at 25°C and a negative thermal coefficient of -4.38×10^{-4}/°C. Thus, the material dispersion of the liquid is fitted by the Cauchy equation [22-23] as $n_{liquid} = A + B/\lambda^2 + C/\lambda^4$, where constants *A*, *B* and *C* are 1.570434, 87857 and 5.1460912 $\times10^8$, respectively. The operation of photonic bandgaps in the *F*-LPCF has been widely reported, where individual high-index inclusions forming isolated waveguides become resonant and finally strongly coupled waveguides at frequencies, whereas forbidden regions appear for spectral ranges, as a result, the fiber is capable of confining and guiding light in the core. It can be seen from Fig. 1(b) that several bandgaps, i.e., G1-G10 are separated by super-modes of the high index inclusions in the *F*-LPCF [20] while G1-G3 are beyond the spectral width under study, though which would help to identify the bandgap number. The lower-order bandgaps (e.g., G5, G6) are located at wide spectral ranges, whereas, the higher-order bandgaps, i.e., G9, G10 present much narrower spectral ranges at shorter wavelengths. According to the Refs. [24, 25], the mode fields supported in the lower-order bandgaps feature more deformation resistant than those of higher-order ones, therefore it is desirable to investigate the first bandgap in the *R*-LPCF.

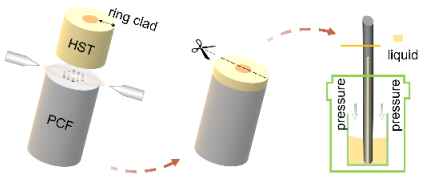

Fig. 2 Schematic diagram of the fabrication process of the proposed *R*-LPCF.

As illustrated in Fig. 2, one end of a conventional PCF is spliced with a hollow silica tube (HST), and then a thin segment of the HST away from the splicing region has been held back by means of a precision cleaving technique. Our simply motivation implies that other air holes of the spliced end of the PCF is fully blocked by the appropriate ring cladding size of the HST except leaving only the first-ring air holes of PCF open. Thus, one end of the selectively opened PCF is sealed in a pressure tube connected to an injection syringe and the other end of the PCF is immerged in a vessel holding for liquid. It's worth noting that our designing scheme just employs a splicer compared with the previously reported method.

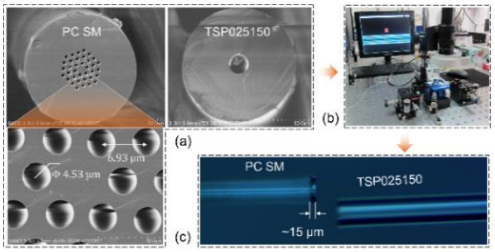

Fig. 3 (a) Scanning electron micrograph (SEM) of the commercial PCF and the HST. The lower-left section depicts the enlarged view. (b) The home-made precision cutting setup. (c) The micrographic procedure.

Followed by the schematic manufacturing procedure of Fig. 2, an index-guiding PCF (PC SM, http://www.yofc.com), and a HST (TSP025150, http://www.innosep.com) are employed, the geometry sizes of which are illustrated in Fig. 3(a). The first-ring holes of the PCF is effectively inside the HST since the holes are located between r_{min} = 6.93 - 4.53/2 = 4.66 μm and r_{max} = 6.93 + 4.53/2 = 9.19 μm, which are lower than 10 μm (the radius of the inner hole of the capillary). In that case some holes in the second ring, which are seated with r_{min} = 2 × 6.93 × cos(pi/6) - 4.53/2 = 9.74 μm, are probably filled. Such size mismatch (9.74 vs. 10 μm) can be addressed through the air holes collapse technique [26], which needs be accomplished in prior to the fabrication of the *R*-LPCF. Given the specifications and models provided from the HST, the proposed method is applicable to the PCFs with the pre-designed ratios (d/Λ). Thus, the manufacturing procedure requires a sophisticated splicing condition and a home-made setup for precision cleaving (Fig. 3(b)). Our previous work [15] in detail illustrated the similar fabrication except the fact that the single mode fiber is replaced with the HST. For instance, the thickness of the residual HST is approximately 15 micros (shown in Fig. 3(c)), which is necessary and convenient for liquid filling.

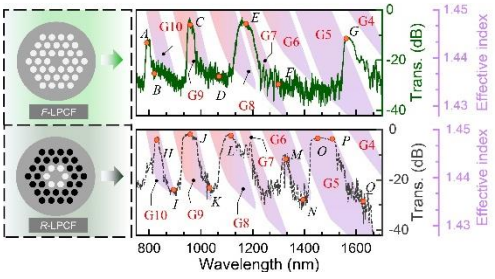

Fig. 4 Measured transmission spectra for the fundamental mode of the *F*-LPCF (Top) and the bandgap-like mode of the *R*-LPCF (Bottom) are plotted in green solid and gray dot lines, respectively. The bandgaps are also indicated.

We employ a supercontinuum source and an optical spectrum analyzer to measure transmission spectra of the *R*-LPCF within the wavelength ranging from 800 nm to 1700 nm. As illustrated in Fig. 4, the transmission spectrum of the *R*-LPCF shows, in general, good qualitative agreement in accordance with that of the *F*-LPCF at short wavelengths. Nonetheless, other new guided windows for the *R*-LPCF occur with the wavelength range of ~1320 to ~1350 nm, ~1427 to ~1517 nm, respectively. It can be explained from the literature [20] that an extra guided core mode for the *R*-LPCF (the contribution of the *7D*-IGF) is obtained at long wavelengths, by contrast, the intensity pattern for the *F*-LPCF core mode begins to couple to cladding modes since the energy begins to locate itself in some high-index inclusions, thereupon this *F*-LPCF core mode disappears in favor of strong coupling with the cladding modes. Furthermore, the transmission spectrum in the *R*-LPCF can give rise to relatively low insertion losses, which are approximately -1.5 dB in the short wavelength (around 900 nm) and -3.2 dB in the long wavelength (around 1500 nm). By contrast, the insertion losses for the *F*-LPCF are higher than -10.8 dB in the 1600-band wavelengths and -4.6 dB in shorter wavelengths. Note that the proposed scheme is quite distinct from the literature [14] since the gold nanoparticles in the aqueous gold colloids play a key part in the loss spectra.

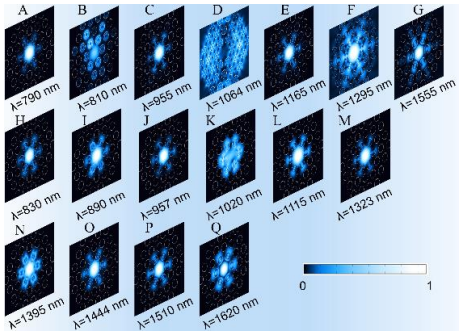

Fig. 5 Intensity patterns of the *F*-LPCF core mode at points (A-G) and the *R*-LPCF bandgap-like core mode at points (H-Q) marked in Fig.4.

In Figs. 5 are also plotted the electric field distributions both for the fundamental mode in the *F*-LPCF and the bandgap-like mode in the *R*-LPCF, which corresponds to the marked points indicated in Fig. 4, respectively. The mode profiles of both fibers are very similar, whereas the bandgap-like mode in the *R*-LPCF exists over a wider spectral range (see the points *A*, *C*, *E*, *G* in the *F*-LPCF, and the points *H*, *J*, *L*, *M*, *O*, *P* in the *R*-LPCF, respectively). According to the Ref. [20], the bandgap-like mode in the *R*-LPCF continue to be guided and extended toward longer wavelength. Besides, the profiles of other points (*B*, *D*, *F*, *I*, *K*, *N*, *Q*) are strongly coupled into the high-index inclusions as a result, energy leaks in the cladding. The point *M* is a mode probably guided in G6 for the *R*-LPCF and does not exist in the *F*-LPCF because only 6 high-index rods exist in the *R*-LPCF, limiting coupling into the cladding. In the *F*-LPCF, edges of bandgaps are too close to the guided mode effective index so in practice there exists high coupling in the cladding and no experimental bandgap probably exists. Moreover, the bandgap-like core mode in the *R*-LPCF exhibits confinement losses (CL) at least 5 orders of magnitude smaller than those of the *F*-LPCF. For instance, the CLs in G and P points are estimated to the order of 10^{-1} dB/m and 10^{-3} dB/km, respectively [27]. It can be attributed to the fact that the bandgap-like core mode in the *R*-LPCF behaves like the fundamental core mode of the *F*-LPCF, also shares the low CL of the core mode guided by the MTIR in the 7DIGF [20].

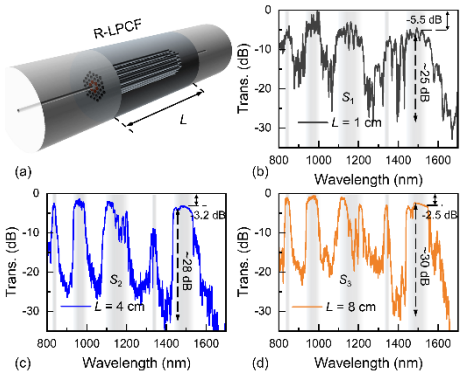

Fig. 6 (a) Schematic diagram of the *R*-LPCF with the infiltrated length *L*. Transmission spectra correspond to (b) *L*=1 cm, (c) *L*=4 cm, (d) *L*=8 cm, respectively.

Thus, the *R*-LPCFs by employing different infiltrated length (S_1, S_2 and S_3) are fabricated, the scheme of which is illustrated in Fig. 6(a). It can be seen from Figs. 6 (b-d) that the transmission spectra with different length present the same bandgap locations, except that the depth of the bandgaps are decreased with the shortened infiltration length due to the fact that the shorter infiltration length does inefficiently match the coupling length of rod modes [15]. In addition, the contrasts between the guided band and the forbidden band are increased with the infiltration length while the insertion losses are reduced with the infiltrated length. In this way, the bandgap contrasts and the insertion losses of the *R*-LPCFs are dependent on the infiltrated length, thus, it requires attaining a balance in the case of our experimental parametric optimization.

Table I Optimized splicing parameters for a commercial fusion splicer (Fujikura-80s)

Parameters	Units	Values
Prefusion power	bit	standard-25
Prefusion time	ms	180
Overlap	μm	6
Fusion power	bit	standard-30
Fusion time	ms	300
Offset	μm	-30

It should be noted that the splicing between the *R*-LPCF and the SMF is challenging so that it requires a sophisticated technique, to conclude a low insertion loss. As shown in Table 1, the parameter 'Offset' plays a key role since the liquid would boil and evaporate under ultrahigh temperature during the fusion splicing, which eventually results in bad physical strength and great splice losses. In our previous works [12, 15, 28], the optimized splicing conditions were grasped through weighing the effects of these parameters after multiple attempts for measuring the transmission spectra. As a result, the splicing losses between the *R*-LPCF and the SMF are probably reduced to be no more than 1.5 dB. On the other hand, the proposed *R*-LPCF corresponds to an analyte volume of approximately one sixth of the *F*-LPCF, as a result, it will further contribute to a low insertion loss as liquids are generally absorptive.

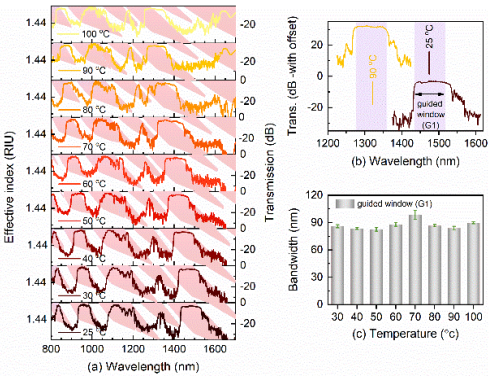

Fig. 7 Transmission spectra and bandgaps (a), the focused guidance spectra (b) and the guided window (c) of the *R*-LPCF in response to the temperature.

Furthermore, as shown in Fig. 7(a), the whole bandgaps shift gradually toward the shorter wavelength with the rising temperature. We mainly focus on investigation of the bandgap (G1) as it covers a broad wavelength, particularly in the 1.5-μm-band communication window, which is shown in Fig. 7(b). It's obviously observed that the guided window (G1) shifts with the temperature without any additional insertion loss, switching from 1.5-μm-band to 1.3-μm-band communication window. And the bandwidth of the window shows no change with the temperature (as shown in Fig. 7(c)), indicating the excellent tunability. Besides, another new low-order bandgap occurs in the long wavelength as the temperature increases.

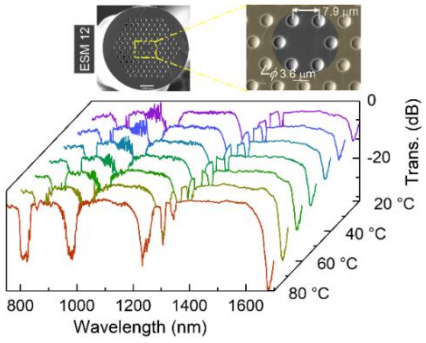

Fig. 8 The measured transmission spectra of another commercial PCF (ESM 12) considered as the ring-pattern selective infiltrated scheme.

As an alternative, a large mode area PCF (ESM-12, http://www.nktphotonics.com) is used to verify the adaptable *R*-LPCF platform. The size of air holes, the period and then the arrangement are obtained from the SEM, which is in the inset of Fig. 8. Here we selected a liquid with a very high refractive index of 1.7 in order to compare with our previously proposed liquid-filled PCF [1]. Obviously, the insertion loss can be reduced to be approximately 3.5 dB while the extinction ratios of bandgaps are more than 40 dB. And the 1500-nm window covers more than 100 nm, which is much wider than those of the previously reported structure [1]. Moreover, the temperature responses of the *R*-LPCF are also investigated, showing a high wavelength tuning sensitivity.

In summary, the proposed *R*-LPCF scheme is employed with two commercial PCFs. Note that only a commercial fusion machine is involved in the fabrication procedure. More significantly, this method can be considered as another selective infiltration technique to develop optical tunable devices.

Funding. The Outstanding Chinese and Foreign Youth Exchange Program of China Association for Science and Technology, the Association Youth Science and Technology Talent Promotion, the 1311 Talents Program of Nanjing University of Posts and Telecommunications (Dingxin), the Marie Skłodowska-Curie Individual Fellowships in the European Union's Horizon 2020 Research and Innovation Programme under Grant 891685.

Disclosures. The authors declare no conflicts of interest.

Acknowledgment. The authors would like to thank the reviewers for their constructive suggestion.

Data availability. Data underlying the results presented in this paper are not publicly available at this time but may be obtained from the authors upon reasonable request.

References

1. Y. Liu, Y. Wang, B. Sun, C. Liao, J. Song, K. Yang, G. Wang, Q. Wang, G. Yin, and J. Zhou, Opt. Lett. 39, 2148 (2014).
2. A. Lorenz, and H.-S. Kitzerow, Appl. Phys. Lett. 98, 241106 (2011).
3. M. Wahle and H.-S. Kitzerow, Opt. Lett. 39, 4816 (2014)
4. H. W. Lee, M. A. Schmidt, and P. St. J. Russell, Opt. Lett. 37, 2946 (2012)
5. H. V. Thakur, S. M. Nalawade, S. Gupta, R. Kitture and S. N. Kale, Appl. Phys. Lett. 99, (2011)
6. P. Zu, C. C. Chan, T. Gong, Y. Jin, W. C. Wong, and X. Dong, Appl. Phys. Lett. 101, 241118 (2012)
7. C. Markos, K. Vlachos, and G. Kakarantzas, IEEE Photon. Technol. Lett. 25, 2003 (2013)
8. I. Konidakis, G. Zito, and S. Pissadakis, Opt. Lett. 37, 2499 (2012)
9. R. Bise, R. Windeler, K. Kranz, C. Kerbage, B. Eggleton, and D. Trevor, Proc. Opt. Fiber Commun. Conf., Anaheim, pp. 466–468, 2002
10. B. T. Kuhlmey, B. J. Eggleton and D. K. C. Wu, Journal of Lightwave Technology, 27(11), 1617-1630 (2009)
11. Y. Wang, X. Tan, W. Jin, D. Ying, Y. L. Hoo, and S. Liu, Opt. Lett. 35, 88-90 (2010)
12. B. Sun, Y. Huang, D. Luo, C. Wang, J. He, C. Liao, G. Yin, J. Zhou, S. Liu, J. Zhao, and Y. Wang, IEEE Photonics J. 7, 6802207-1 (2015)
13. F. Wang, W. Yuan, O. Hansen, and O. Bang, Opt. Express 19, 17585 (2011)
14. Y. Peng, J. Hou, Y. Zhang, Z. Huang, R. Xiao, and Q. Lu, Opt. Lett. 38, 263 (2013)
15. B. Sun, Z. Zhang, W. Wei, C. Wang, C. Liao, L. Zhang, and Y. Wang, IEEE Photonics Technol. Lett. 28(12), 1282–1285 (2016)
16. Y. Huang, Ying Wang, Longfei Zhang, Yu Shao, Feng Zhang, Changrui Liao, Yiping, Journal of Lightwave Technology 37, 1903 (2019)
17. M. Luo, Y. Liu, Z. Wang, T. Han, Z. Wu, J. Guo, and W. Huang, Opt. Express 21, 30911 (2013)
18. Stephen C. Warren-Smith, Ricardo M. André, Christopher Perrella, Jan Dellith, and Hartmut Bartelt, Opt. Express 24, 378-387 (2016).
19. S. Ertman, K. Rutkowska and T. R. Woliński, Journal of Lightwave Technology, vol. 37 2516 (2019)
20. Y. Agha, A. Bétourné, O. Vanvincq, G. Bouwmans, and Y. Quiquempois, Opt. Express 20, 6746-6760 (2012)
21. I. Malitson, J. Opt. Soc. Am. 55(10), 1205–1208 (1965)
22. M. Luo, Y. Liu, Z. Wang, T. Han, Z. Wu, J. Guo, and W. Huang, Opt. Express 21, 30911-30917 (2013)
23. https://www.cargille.com
24. Guobin Ren, Ping Shum, Liren Zhang, Xia Yu, Weijun Tong, and Jie Luo, Opt. Lett. 32, 1023-1025 (2007)
25. A. Argyros, T. A. Birks, S. G. Leon-Saval, C. M. B. Cordeiro, and P. St.J. Russell, Opt. Express 13, 2503-2511 (2005)
26. L. Xiao, W. Jin, M. Demokan, H. Ho, Yeuk L. Hoo, and C. Zhao, Opt. Express 13, 9014-9022 (2005)
27. J. Han, E. Liu, and J. Liu, J. Opt. Soc. Am. A 36, 533-539 (2019)

References

1. Y. Liu, Y. Wang, B. Sun, C. Liao, J. Song, K. Yang, G. Wang, Q. Wang, G. Yin, and J. Zhou, “Compact tunable multibandpass filters based on liquid-filled photonic crystal fibers,” Opt. Lett. 39, 2148 (2014).
2. A. Lorenz, and H.-S. Kitzerow, “Efficient electro-optic switching in a photonic liquid crystal fiber,” Appl. Phys. Lett. 98, 241106 (2011).
3. M. Wahle and H.-S. Kitzerow, “Measurement of group velocity dispersion in a solid-core photonic crystal fiber filled with a nematic liquid crystal,” Opt. Lett. 39, 4816 (2014).
4. H. W. Lee, M. A. Schmidt, and P. St. J. Russell, “Excitation of a nanowire ‘molecule’ in gold-filled photonic crystal fiber,” Opt. Lett. 37, 2946 (2012).
5. H. V. Thakur, S. M. Nalawade, S. Gupta, R. Kitture and S. N. Kale, “Photonic crystal fiber injected with Fe3O4 nanofluid for magnetic field detection,” Appl. Phys. Lett. 99, (2011).
6. P. Zu, C. C. Chan, T. Gong, Y. Jin, W. C. Wong, and X. Dong, “Magneto-optical fiber sensor based on bandgap effect of photonic crystal fiber infiltrated with magnetic fluid,” Appl. Phys. Lett. 101, 241118 (2012).
7. C. Markos, K. Vlachos, and G. Kakarantzas, “Broadband guidance in a hollow-core photonic crystal fiber with polymer-filled cladding,” IEEE Photon. Technol. Lett. 25, 2003 (2013).
8. I. Konidakis, G. Zito, and S. Pissadakis, “Photosensitive, all-glass AgPO3/silica photonic bandgap fiber,” Opt. Lett. 37, 2499 (2012).
9. R. T. Bise, R. S.Windeler, K. S. Kranz, C. Kerbage, B. J. Eggleton, and D. J. Trevor, “Tunable photonic band gap fiber,” in Proc. Opt. Fiber Commun. Conf. (OFC), Anaheim, CA, 2002, pp. 466–468.
10. B. T. Kuhlmey, B. J. Eggleton and D. K. C. Wu, "Fluid-Filled Solid-Core Photonic Bandgap Fibers," Journal of Lightwave Technology, vol. 27, no. 11, pp. 1617-1630, June1, 2009
11. Y. Wang, X. Tan, W. Jin, D. Ying, Y. L. Hoo, and S. Liu, "Temperature-controlled transformation in fiber types of fluid-filled photonic crystal fibers and applications," Opt. Lett. 35, 88-90 (2010).
12. B. Sun, Y. Huang, D. Luo, C. Wang, J. He, C. Liao, G. Yin, J. Zhou, S. Liu, J. Zhao, and Y. Wang, “Broadband Thermo-Optic Switching Effect Based on Liquid Crystal Infiltrated Photonic Crystal Fibers,” IEEE Photonics J. 7, 6802207-1 (2015).
13. F. Wang, W. Yuan, O. Hansen, and O. Bang, “Selective filling of photonic crystal fibers using focused ion beam milled microchannels,” Opt. Express 19, 17585 (2011).
14. Y. Peng, J. Hou, Y. Zhang, Z. Huang, R. Xiao, and Q. Lu, "Temperature sensing using the bandgap-like effect in a selectively liquid-filled photonic crystal fiber," Opt. Lett. 38, 263 (2013)
15. B. Sun, Z. Zhang, W. Wei, C. Wang, C. Liao, L. Zhang, and Y. Wang, “Unique temperature dependence of selectively liquid-crystal-filled photonic crystal fibers,” IEEE Photonics Technol. Lett. 28(12), 1282–1285 (2016)
16. Y. Huang, Ying Wang, Longfei Zhang, Yu Shao, Feng Zhang, Changrui Liao, Yiping Wang "Tunable electro-optical modulator based on a photonic crystal fiber selectively filled with liquid crystal," Journal of Lightwave Technology 37, 1903 (2019).
17. M. Luo, Y. Liu, Z. Wang, T. Han, Z. Wu, J. Guo, and W. Huang, "Twin-resonance-coupling and high sensitivity sensing characteristics of a selectively fluid-filled microstructured optical fiber," Opt. Express 21, 30911 (2013).
18. Stephen C. Warren-Smith, Ricardo M. André, Christopher Perrella, Jan Dellith, and Hartmut Bartelt, "Direct core structuring of microstructured optical fibers using focused ion beam milling," Opt. Express 24, 378-387 (2016).
19. S. Ertman, K. Rutkowska and T. R. Woliński, "Recent Progress in Liquid-Crystal Optical Fibers and Their Applications in Photonics," Journal of Lightwave Technology, vol. 37 2516 (2019)
20. Y. Agha, A. Bétourné, O. Vanvincq, G. Bouwmans, and Y. Quiquempois, “Broadband bandgap guidance and mode filtering in radially hybrid photonic crystal fiber,” Opt. Express 20, 6746-6760 (2012)
21. I. Malitson, “Interspecimen comparison of the refractive index of fused silica,” J. Opt. Soc. Am. 55(10), 1205–1208 (1965)
22. M. Luo, Y. Liu, Z. Wang, T. Han, Z. Wu, J. Guo, and W. Huang, “Twin-resonance-coupling and high sensitivity sensing characteristics of a selectively fluid-filled microstructured optical fiber,” Opt. Express 21, 30911-30917 (2013)
23. https://www.cargille.com
24. Guobin Ren, Ping Shum, Liren Zhang, Xia Yu, Weijun Tong, and Jie Luo, "Low-loss all-solid photonic bandgap fiber," Opt. Lett. 32, 1023-1025 (2007)
25. A. Argyros, T. A. Birks, S. G. Leon-Saval, C. M. B. Cordeiro, and P. St.J. Russell, "Guidance properties of low-contrast photonic bandgap fibres," Opt. Express 13, 2503-2511 (2005)
26. L. Xiao, W. Jin, M. Demokan, H. Ho, Yeuk L. Hoo, and C. Zhao, "Fabrication of selective injection microstructured optical fibers with a conventional fusion splicer," Opt. Express 13, 9014-9022 (2005)
27. J. Han, E. Liu, and J. Liu, "Circular gradient-diameter photonic crystal fiber with large mode area and low bending loss," J. Opt. Soc. Am. A 36, 533-539 (2019)